Electronic Supplementary Material (ESI) for Inorganic Chemistry Frontiers.

Supplementary information

The role of terminal ligands on the slow relaxation of magnetization and luminescence thermometry of dinuclear Nd^{III} complexes

Airton G. Bispo-Jr, Diogo A. Gálico, Roberto M. Diaz-Rodriguez, Jeffrey S. Ovens, Fernando A. Sigoli,* Muralee Murugesu*

Contents

Supplementary Note S1 – Experimental Procedures

Synthesis

H_2valdien proligand. H_2valdien (*N*¹,*N*³-bis(3-methoxysalicylidene)diethylenetriamine) was obtained from the condensation of *o*-vanillin (TCI America, 99.0%) and diethylenetriamine (Sigma-Aldrich, 99%) as described in reference 1.

[Nd_2(valdien)$_2$(acac)$_2$] ({1-Nd_2}). H_2valdien (0.250 mmol, 0.092 g) and [Nd(acac)$_3$(H_2O)$_2$] (Sigma-Aldrich, 99%, 0.250 mmol, 0.124 g) were dissolved in 9 mL of MeOH/DMF (2:1 v/v). Triethylamine (Fisher Chemical, 99%, 0.500 mmol, 70 µL) was then added; the yellow solution was stirred for 5 min, then filtered. Rectangular-shaped yellow crystals were obtained after one day by diffusion of diethyl ether vapour into the filtrate at room temperature. IR (Fig. S1): $\bar{\nu} =$ 2869 (w), 1658 (s), 1603 (s), 1515 (m), 1440 (m), 1386 (s), 1326 (m), 1270 (m), 1237 (s), 1212 (s), 1091 (s), 915 (m), 852 (m), 786 (w), 746 (s), 659 (m) cm^{-1}.[1] Anal. Calcd (%) for $C_{50}H_{60}N_6Nd_2O_{12}$ (1225.52 g mol^{-1}): C, 49.00; H, 6.86; N, 4.41. Found: C, 49.60; H, 4.41; N, 7.01.

[Nd_2(valdien)$_2$(NO_3)$_2$] ({2-Nd_2}). A solution of triethylamine (0.500 mmol, 70 µL) and Nd(NO_3)$_3$·6H_2O (Sigma-Aldrich, 99%, 0.250 mmol) in 4 mL of MeOH/CH_2Cl_2 (1:1 v/v) was added to a solution of H_2valdien (0.250 mmol, 0.092 g) in 5 mL of MeOH/CH_2Cl_2 (1:1 v/v). The resulting yellow solution was stirred for 5 min and then filtered. Crystals were grown in the same way as described above for **{1-Nd_2}**. IR (Fig. S1): $\bar{\nu} =$ 3208 (m), 2906 (m), 1635 (m), 1617 (s), 1546 (w), 1489 (m), 1465 (m), 1436 (s), 1400 (m), 1384 (s), 1349 (w), 1323 (m), 1271 (m), 1240 (s), 1215 (m), 1167 (w), 1106 (w), 1076 (m), 1039 (w), 997 (w), 968 (m), 916 (w), 853 (w), 735 (s), 621 (w) cm^{-1}.[1] Anal. Calcd (%) for $C_{40}H_{46}N_8Nd_2O_{14}$ (1151.33 g mol^{-1}): C, 41.66; H, 4.02; N, 8/80. Found: C, 39.20; H, 4.04; N, 11.13.

Characterization

Single-crystal X-ray diffraction. Crystallographic data were collected from single crystals mounted on MiTeGen MicroMounts using Parabar 10312 oil. Data were collected using Bruker AXS APEX II KAPPA or SMART single crystal diffractometers equipped with sealed tube Mo Kα sources (λ= 0.71073 Å), graphite monochromators, and APEX II CCD detectors. Raw data collection and processing were performed with the APEX II software package from Bruker.[2] Initial unit cell parameters were determined using 36 data frames from selected ω scans. Semi-empirical absorption corrections based on equivalent reflections were applied.[3] Systematic absences in the diffraction dataset and unit cell parameters were consistent with the assigned space group. The initial structural solutions were determined using ShelXT direct methods,[4] and refined with full-matrix least-squares procedures based on F^2 using ShelXL and ShelXle.[5] Hydrogen atoms were placed geometrically and refined using a riding model. Twinning in **{2-Nd_2}** was determined via PLATON, and subsequently refined in ShelXle.

Infrared spectroscopy. Fourier transform infrared (FTIR) spectra were recorded in the $\tilde{\nu}$ = 4000-525 cm^{-1} range using a Nicolet 6700 FTIR spectrometer equipped with an attenuated total reflectance (ATR) attachment.

Photoluminescence. All photoluminescence data were obtained for powdered samples using a Horiba QuantaMaster 8075-21 spectrofluorometer equipped with a liquid-nitrogen-cooled InGaAs detector for the near-infrared range (900 – 1550 nm). An ozone-free PowerArc 75 W xenon lamp was used as the radiation source. The emission spectra were corrected according to the optical system of the emission monochromator and the detector response.

For temperature-dependent luminescence, excitation and emission spectra from 10 K to 330 K were measured. To control the temperature, a Janis CCS-100/204N cryostat with an Acme Electric T181059 compressor and a LakeShore 335 temperature controller were used. The relative thermal sensitivity S_r is calculated from eqn S1, where Δ is the thermometric parameter and T is the temperature. The temperature uncertainty δT is calculated using eqn S2, where $\delta I/I$ is the relative uncertainty in the integrated area.[6]

$$S_r = \frac{1}{\Delta}\left|\frac{d\Delta}{dT}\right| \qquad (S1)$$

$$\delta T = \frac{1}{S_r}\frac{\delta\Delta}{\Delta} \qquad (S2)$$

$$\frac{\delta\Delta}{\Delta} = \sqrt{\left(\frac{\delta I_1}{I_1}\right)^2 + \left(\frac{\delta I_2}{I_2}\right)^2} \qquad (S3)$$

Magnetometry. Magnetic measurements were performed using a Quantum Design PPMS Dynacool-14T physical property measurement system equipped with a vibrating sample magnetometer (VSM), operating between 1.8 and 300 K. DC and AC measurements were performed on a crushed polycrystalline sample of 27.1 mg for **{1-Nd_2}** and 33.0 mg for **{2-Nd_2}**. Both samples analyzed here come from the same batch where bulk purity was confirmed through, PXRD, elemental analysis and IR spectroscopy. The samples were restrained in a matrix of vacuum grease (Corning) and wrapped in a polyethylene membrane. The magnetization data were collected at 100 K to check for ferromagnetic impurities, which were absent in both samples. Diamagnetic corrections were applied for the sample holder, and the inherent diamagnetism of the samples was estimated with the use of Pascal's constants.

Supplementary Note S2 – Infrared Spectra

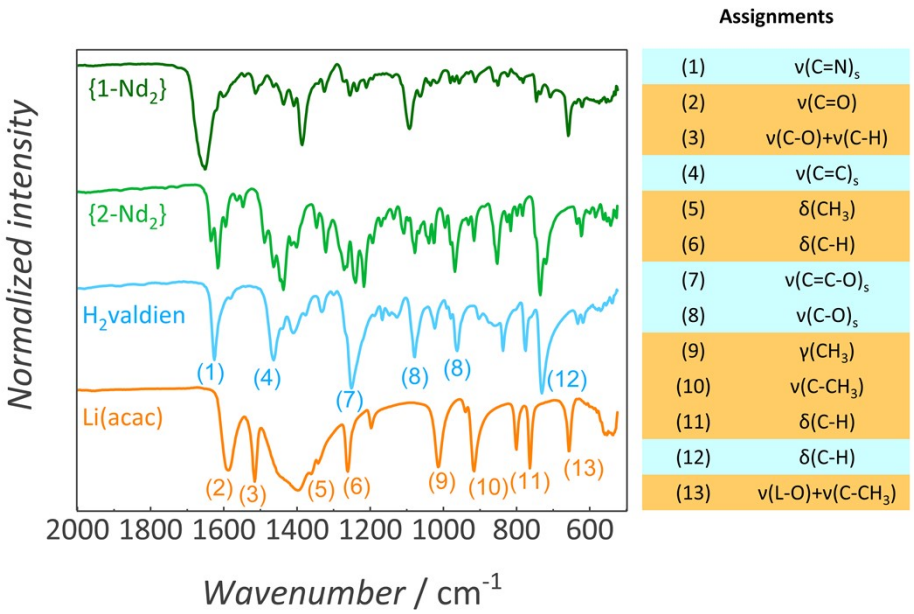

Fig. S1. FTIR spectra (293 K) of **{1-Nd_2}** and **{2-Nd_2}** crushed crystals compared to powder H_2valdien and Li(acac). On the right, assignments of the H_2valdien vibrational modes are highlighted in light blue and those of Li(acac) in orange.

Supplementary Note S3 – Structural Analyses

Table S1. Crystallographic data for **{1-Nd_2}** and **{2-Nd_2}**.

	{1-Nd_2}	**{2-Nd_2}**
CCDC deposition number	2242690	2242689
Temperature, K	273	200
Empirical formula	$C_{50}H_{60}N_6Nd_2O_{12}$	$C_{40}H_{46}N_8Nd_2O_{14}$
Molecular weight, g mol^{-1}	1225.52	1151.33
Radiation (wavelength, Å)	Mo Kα (0.71073)	Mo Kα (0.71073)
Crystal system	Monoclinic	Monoclinic
Space group	$P2_1/n$	$P2_1/c$
a, Å	12.4641(10)	22.5475(9)
b, Å	10.6436(8)	10.3176(4)
c, Å	18.7115(16)	20.0493(8)
α, °	90	90
β, °	95.694(3)	112.018(2)
γ, °	90	90
Volume	2470.1(3)	4324.0(3)
Z	2	4
Density (*ρ*), g cm^{-3} calc'd.	1.648	1.769
μ, mm^{-1}	2.147	2.451
F(0 0 0)	1236.0	2296.0
Crystal size, mm^3	0.019 x 0.169 x 0.25	0.077 x 0.095 x 0.109
Theta range, °	1.880 - 26.410	1.949 - 26.629
Index ranges (h,k,l)	(15 13 23)	(27 12 25)
No. of reflections measured	5067	8990
No. of independent reflections	3199	5697
R(int)	0.092	-
Completeness, %	0.998	0.989
Max. and min. transmission	0.7454 / 0.6199	0.745 / 0.694
Data / restraints / parameters	5067 / 0 / 320	8990 / 632 / 582
R_1, wR_2 ($I > 2\sigma(I)$)[a]	0.0562, 0.1063	0.0597, 0.1231
R_1, wR_2 (all data)	0.1085, 0.1220	0.1101, 0.1417
Goodness of fit on F^2	1.028	1.044
Largest differential peak and hole, $e^-/Å^3$	1.62 / -1.13	1.583 / -2.440

[a] $$R = R_1 = \sum \frac{||F_0| - |F_c||}{\sum |F_0|}$$

$$wR_2 = \left\{\sum \left[w(F_0^2 - F_c^2)^2\right] / \sum \left[w(F_0)^2\right]\right\}^{1/2}$$

Where $w = 1/\left[\sigma\left(F_0^2\right) + (ap)^2 + bp\right]$

$$p = [max(F_0^2, 0)] + 2F_c^2]/3$$

$$R_w = [w(|F_0| - |F_c|)^2 / w|F_0|^2]^{1/2}$$

Where $w = 1/\sigma^2(|F_0|)$

Table S2. Intramolecular H-bond distance, intramolecular Nd – Nd distance, shortest intermolecular Nd ⋯ Nd distance, and Nd - O - Nd angle in **{1-Nd$_2$}** and **{2-Nd$_2$}**.

	H-bond / Å	Nd - Nd / Å	Nd ⋯ Nd / Å	Nd - O - Nd / °
{1-Nd$_2$}	1.98(4)	4.0732(6)	9.093(9)	110.14(14)
{2-Nd$_2$}	1.95(7)	3.9364(7)	8.619(8)	108.59(12)

Table S3. Selected Nd – O and Nd – N distances in **{1-Nd$_2$}** and **{2-Nd$_2$}**.

{1-Nd$_2$}		**{2-Nd$_2$}**	
Bond	**Distance / Å**	**Bond**	**Distance / Å**
Nd – O5*	2.4133(52)	Nd – O12*	2.5509(73)
Nd – O6*	2.4173(49)	Nd – O14*	2.5372(10)
Nd – O3**	2.4665(37)	Nd – O9**	2.4031(68)
Nd – O3'**	2.5014(41)	Nd – O9'**	2.4444(68)
Nd – O2	2.2780(51)	Nd – O11	2.4792(68)
Nd – N1	2.6398(62)	Nd – N5	2.6202(70)
Nd – N2	2.6488(53)	Nd – N6	2.5833(83)
Nd – N3	2.6698(58)	Nd – N7	2.6184(74)

*Nd – O_{term}. **Nd – O_{core}.

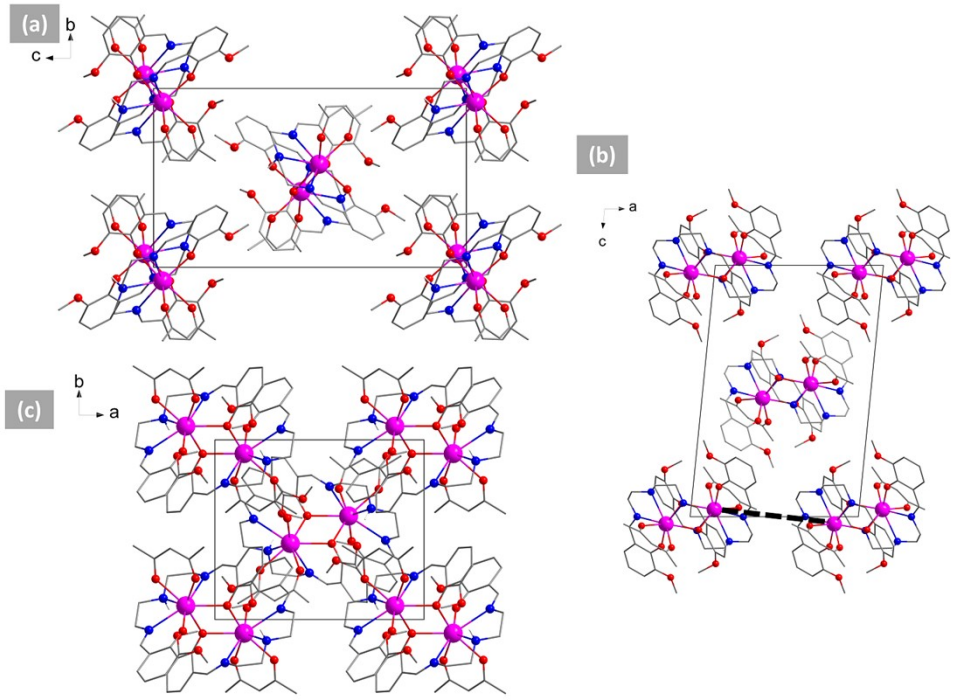

Fig. S2. View of the packing arrangement along the crystallographic (a) *a*, (b) *b*, and (c) *c*-axis in **{1-Nd$_2$}**. The black dashed line represents the shortest Nd – Nd intermolecular distance. Hydrogen atoms are omitted for clarity.

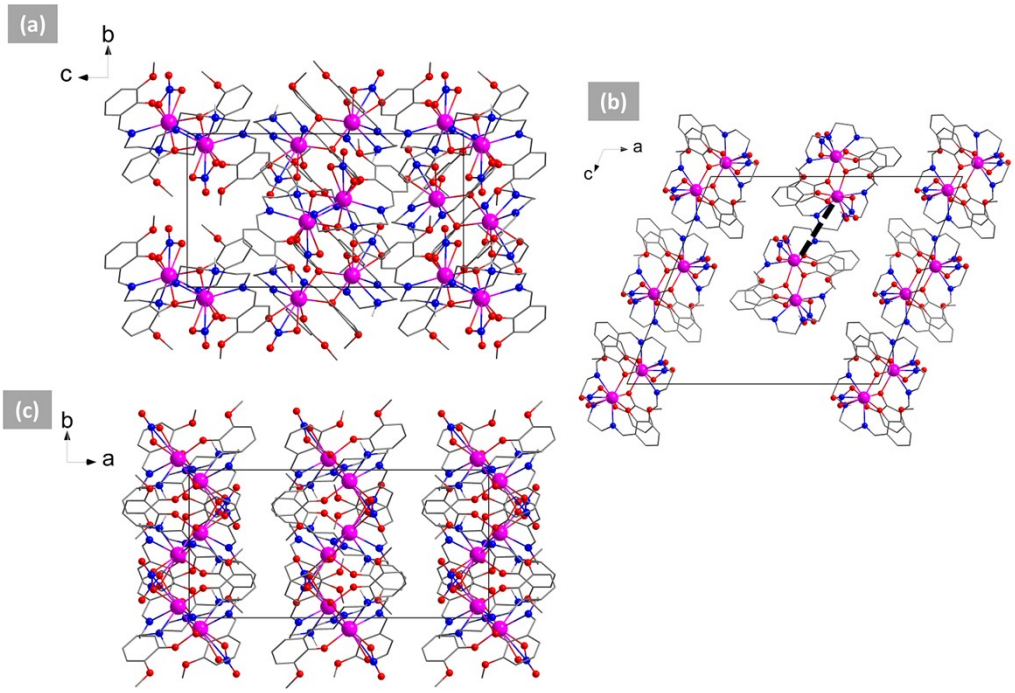

Fig. S3. View of the packing arrangement along the crystallographic (a) *a*, (b) *b*, and (c) *c*-axis in **{2-Nd$_2$}**. The black dashed line represents the shortest Nd – Nd intermolecular distance. Hydrogen atoms are omitted for clarity.

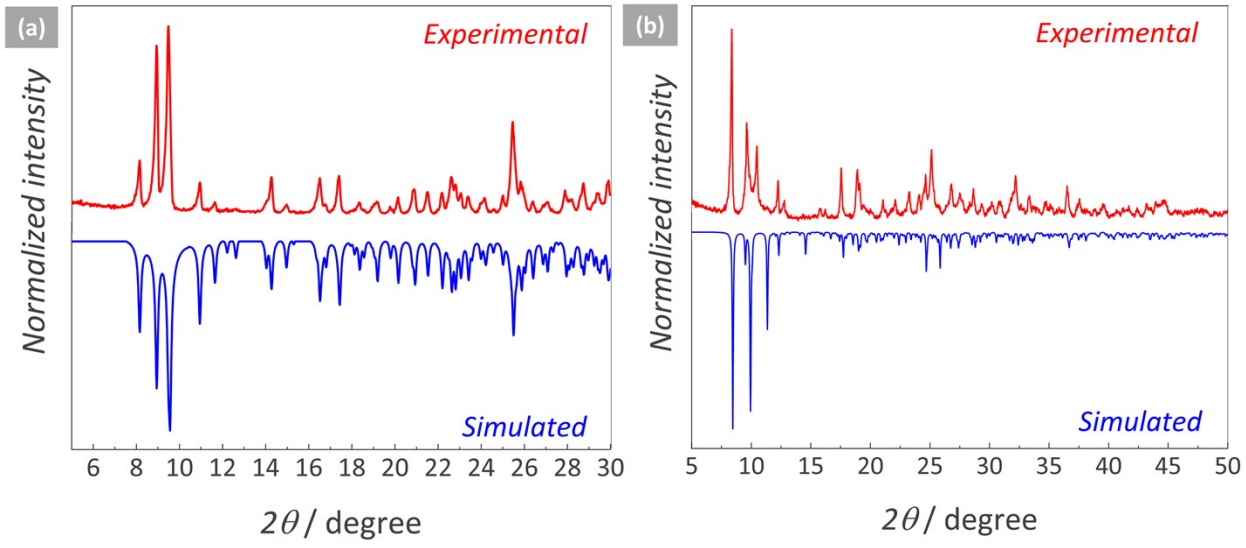

Fig. S4. Powder X-ray diffractograms of (a) **{1-Nd$_2$}** and (b) **{2-Nd$_2$}** compared to the simulated patterns determined from the single-crystal structures.

Supplementary Note S4 – Additional Magnetic Data

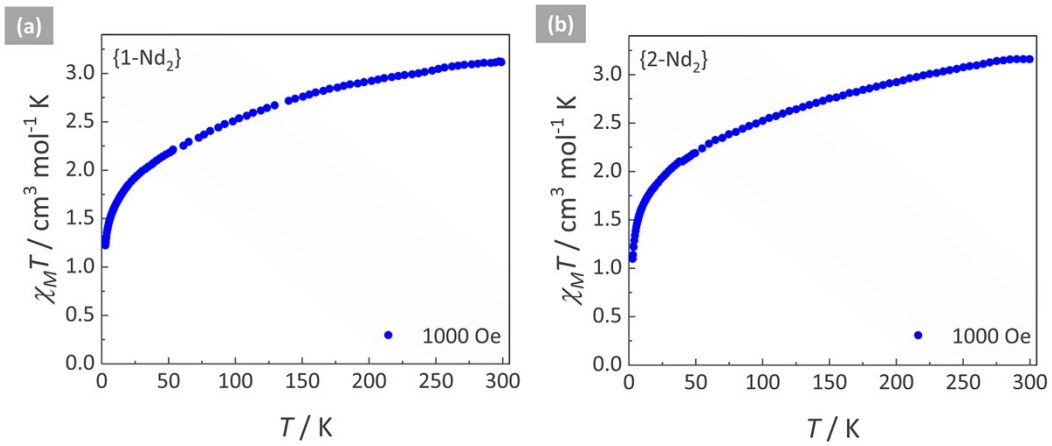

Fig. S5. Temperature dependence of the $\chi_M T$ product under an applied field of 1000 Oe for **{1-Nd$_2$}** and **{2-Nd$_2$}**, with χ_M being the molar magnetic susceptibility per molecule, defined as *M/H*.

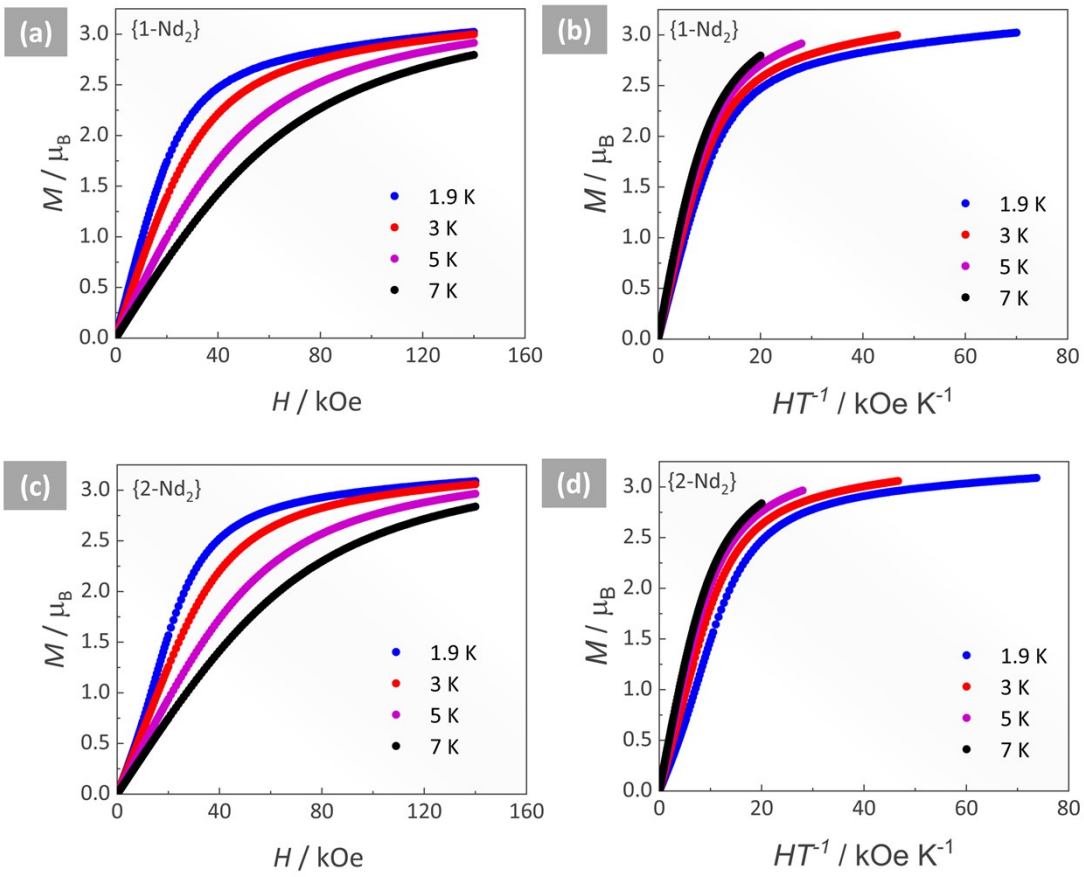

Fig. S6. Isothermal field dependence of the magnetization ((a) and (c)) and the reduced magnetization HT^{-1} ((b) and (d)) at the indicated temperatures for **{1-Nd$_2$}** and **{2-Nd$_2$}**. The obtained data reveal that in the magnetization (M vs. H) and reduced magnetization (M vs. HT 1) plots, the magnetization increases as temperature decreases and the magnetic field increases, whose maximum is achieved at 3.02 μB (1.9 K), 2.99 μB (3.0 K), 2.91 μB (5.0 K), and 2.79 μB (7 K) for {1-Nd2} and at 3.09 μB (1.9 K), 3.06 μB (3.0 K), 2.97 μB (5.0 K), and 2.84 μB (7 K) for {2-Nd2}.

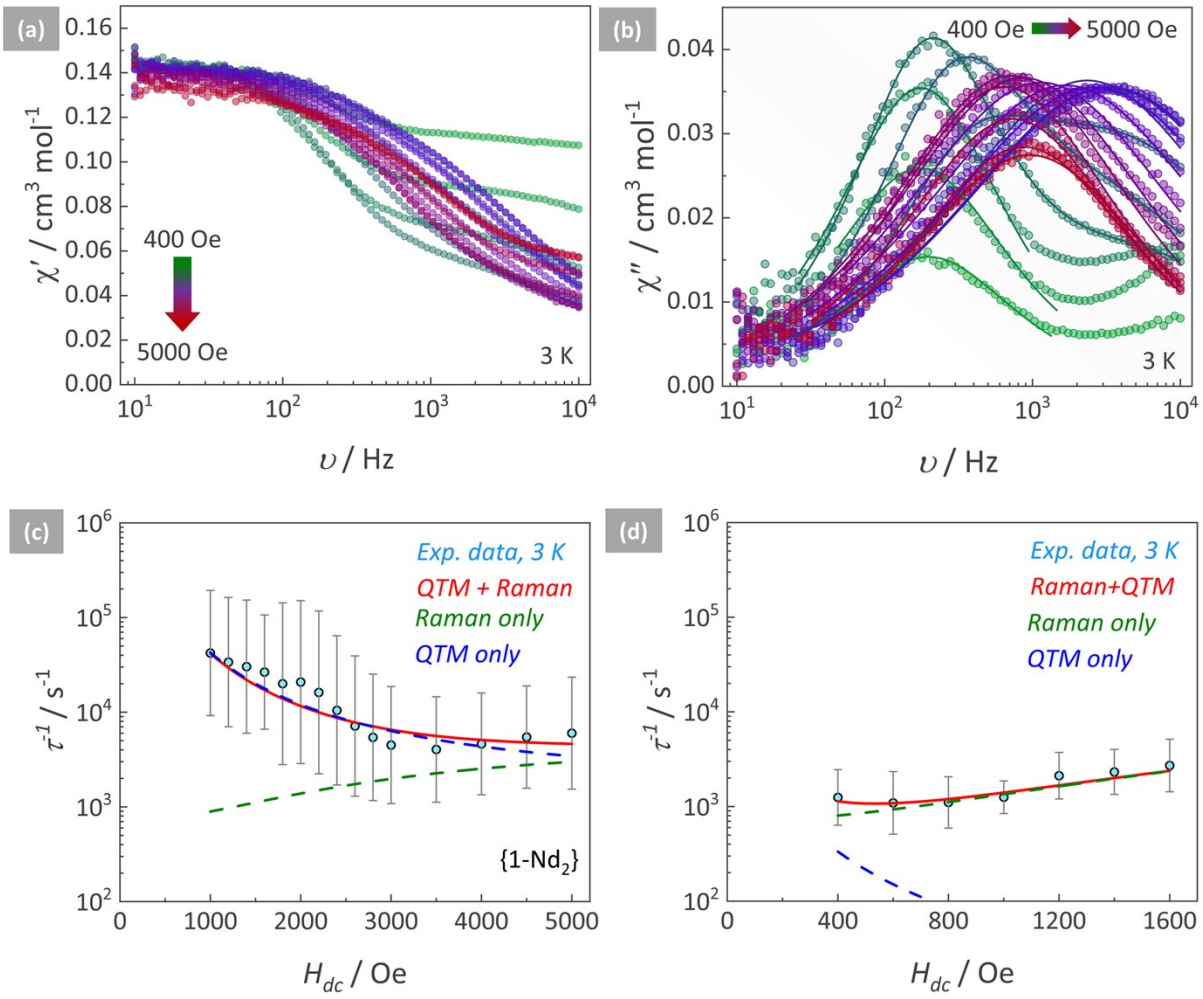

Fig. S7. Frequency dependence of the (a) in-phase (χ') and (b) out-of-phase (χ'') molar magnetic susceptibility as a function of applied field H_{dc} from 400 Oe to 5000 Oe at 3 K for **{1-Nd$_2$}**. The solid lines in (b) represent fits to the single (H_{dc} = 400 – 800 Oe, 1800 – 4500 Oe) or double (H_{dc} = 1000 - 1600 Oe) Debye model, with best-fitting parameters given in Table S4. For the curves obtained at 400, 600, and 800 Oe, although a tailing component is noticed in the high-frequency region, the peak maximum is out of range, thus a single Debye model was applied considering only the main observed component. Field dependence of the relaxation time of magnetization (τ) at 3 K for the (b) high-frequency (HF) and (c) low-frequency (LF) processes. The solid lines represent the best fit according to eqn 1, with parameters given in Table S5.

Table S4. Best-fitting parameters of the generalized single or double Debye model for the frequency dependence of the out-of-phase molar magnetic susceptibility (χ'') as a function of applied field (H_{dc}) at 3 K for **{1-Nd$_2$}**.

H_{dc} / Oe	χ_s / cm^3 mol^{-1}	χ_t / cm^3 mol^{-1}	α	τ / s	χ_s / cm^3 mol^{-1}	χ_t / cm^3 mol^{-1}	α	τ / s
400					0.00674	0.04326	0.1093	8.02042E-4
600					6.79243E-4	0.06453	0.13181	9.15881E-4
800					2.01801E-5	0.08242	0.09596	9.04955E-4
1000	0.00212	0.04727	0.32194	2.36914E-5	0	0.08136	0.04357	7.9746E-4
1200	0.00443	0.06325	0.33243	2.95706E-5	0	0.07147	0.08144	4.72736E-4
1400	0.00405	0.09477	0.34235	3.2983E-5	0.01652	0.05885	0.0768	4.31072E-4
1600	0.00111	0.10151	0.2919	3.76614E-5	0	0.03018	0.0995	3.68732E-4
1800	1.63826E-4	0.14172	0.40851	4.99457E-5				
2000	8.91324E-4	0.14322	0.41104	4.79975E-5				
2200	9.01585E-4	0.14319	0.41076	6.17505E-5				
2400	6.28609E-5	0.13543	0.38124	9.54981E-5				
2600	6.63461E-5	0.1313	0.35991	1.39861E-4				
2800	9.00882E-4	0.12592	0.32523	1.84095E-4				
3000	0.0011	0.12146	0.29972	2.22174E-4				
3500	0.00178	0.1113	0.26684	2.47231E-4				
4000	3.4885E-4	0.09632	0.25602	2.15965E-4				
4500	1.04905E-4	0.08624	0.25725	1.8288E-4				
5000	5.32287E-4	0.08795	0.28589	1.66275E-4				

Table S5. Summary of the best-fitting parameters of the field dependence of the relaxation time of magnetization (τ) for **{1-Nd$_2$}** at 3 K. HF = high frequency, LF = low frequency.

Mechanism	Parameter	HF process	LF process
QTM	*B1*	1.30 10^4 s^{-1}	3.32 10^{10} s^{-1}
	B2	2.48 10^{-4} Oe^{-2}	0.81 Oe^{-2}
Raman	*C*	0.051 s^{-1} K^{-n}	0.051 s^{-1} K^{-n}
	C1	9.30 10^{-7} Oe^{-2}	3.45 10^{-7} Oe^{-2}
	C2	0	4.99 10^{-8} Oe^{-2}
	n	8.66	8.66

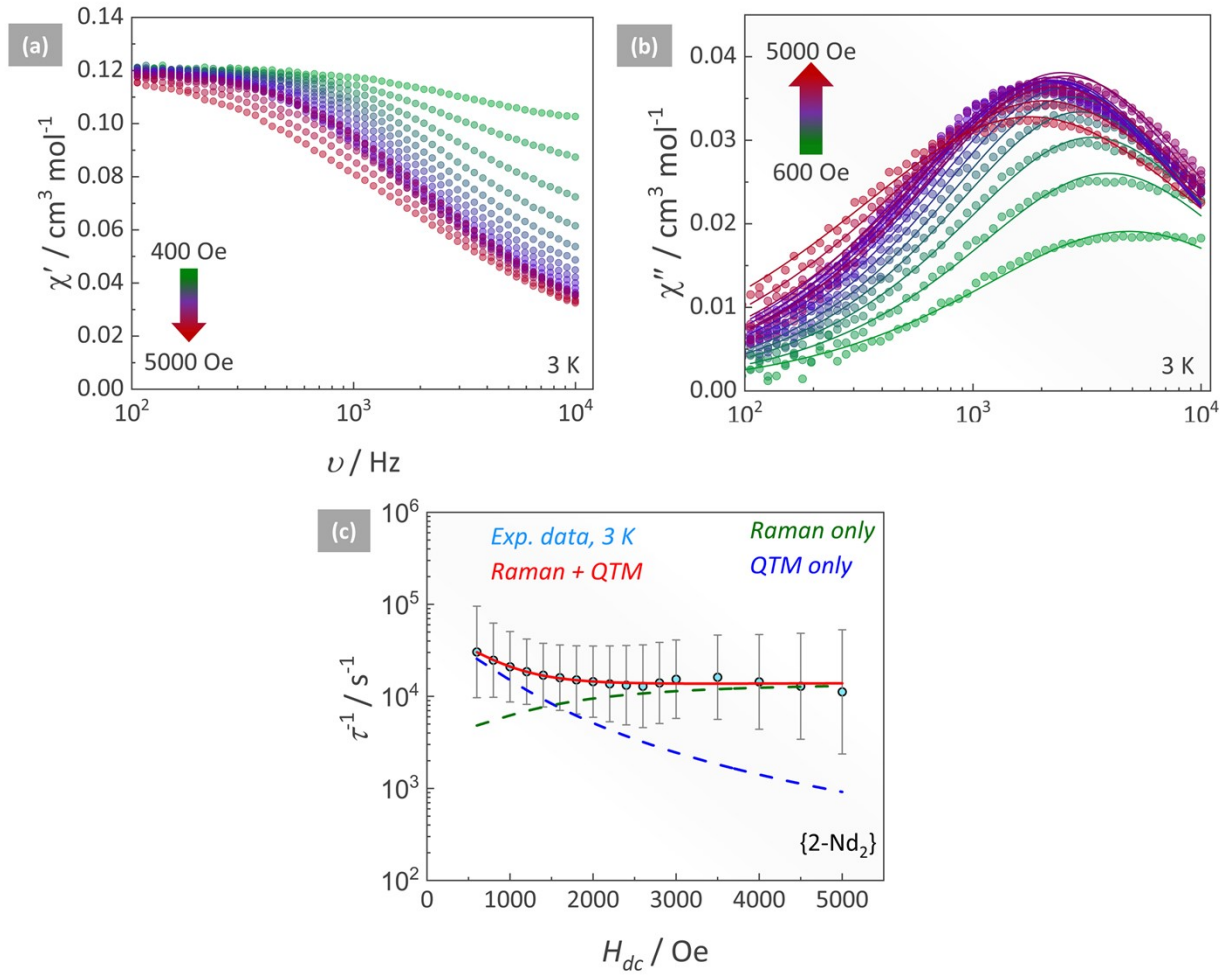

Fig. S8. (a) Frequency dependence of the out-of-phase molar magnetic susceptibility (χ'') as a function of applied field H_{dc} from 600 Oe to 5000 Oe at 3 K for **{2-Nd$_2$}**. The solid lines represent fits to the single Debye model, with parameters given in Table S6. (b) Field dependence of the relaxation time of magnetization (τ) at 3 K. The solid lines represent the best fit to the QTM and Raman processes according to eqn 1, with parameters given in Table S7.

Table S6. Best-fitting parameters of the generalized single Debye model for the frequency dependence of the out-of-phase molar magnetic susceptibility (χ'') as a function of applied field H_{dc} at 3 K for **{2-Nd$_2$}**.

H_{dc} / Oe	χ_s / cm^3 mol^{-1}	χ_t / cm^3 mol^{-1}	α	τ / s
600	0.00964	0.06513	0.23275	3.28722E-5
800	0.23276	0.30173	0.17658	4.04311E-5
1000	0.23032	0.30903	0.16383	4.76292E-5
1200	0.27234	0.3566	0.14684	5.38585E-5
1400	0.15601	0.24399	0.14124	5.87928E-5
1600	0.00421	0.09579	0.14711	6.25654E-5
1800	9.25971E-7	0.0946	0.15662	6.62278E-5
2000	0.00212	0.09892	0.16668	6.91059E-5
2200	2.7887E-6	0.09928	0.18167	7.30589E-5
2400	2.56307E-4	0.10125	0.1939	7.55534E-5
2600	4.12469E-4	0.10306	0.20472	7.7507E-5
2800	6.33052E-5	0.10324	0.19936	7.14269E-5
3000	7.73523E-5	0.10329	0.1904	6.508E-5
3500	4.2872E-5	0.10544	0.20962	6.19151E-5
4000	1.2769E-5	0.10745	0.24287	6.95402E-5
4500	1.11431E-4	0.109	0.27721	7.76062E-5
5000	8.9449E-4	0.11356	0.32872	8.9287E-5

Table S7. Summary of the best-fitting parameters of the field dependence of the relaxation time of magnetization (τ) for **{2-Nd$_2$}** at 3 K.

Mechanism	Parameter	Value
QTM	*B1*	4.21 10^4 s^{-1}
	B2	1.82 10^{-6} T^{-2}
Raman	*C*	56.8 s^{-1} K^{-n}
	C1	1.11 10^{-6} Oe^{-2}
	C2	2.93 10^{-7} Oe^{-2}
	n	3.83

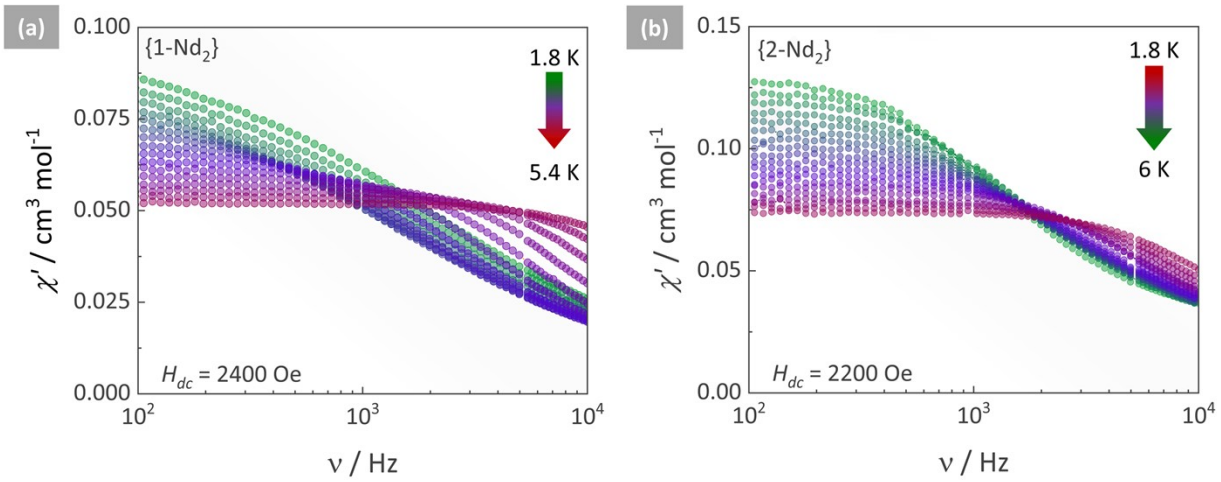

Fig. S9. Frequency dependence of the in-phase molar magnetic susceptibility (χ') as a function of temperature for (a) **{1-Nd$_2$}** (H_{dc} = 2400 Oe) and (b) **{2-Nd$_2$}** (H_{dc} = 2200 Oe).

Table S8. Best-fitting parameters of the generalized single Debye model for the frequency dependence of the out-of-phase molar magnetic susceptibility (χ'') as a function of temperature for **{1-Nd$_2$}** (H_{dc} = 2400 Oe).

T / K	χ_s / cm^3 mol^{-1}	χ_t / cm^3 mol^{-1}	α	τ / s
1.8	8.16633E-5	0.10864	0.42269	8.61915E-5
2	1.8089E-4	0.10308	0.42569	8.46894E-5
2.2	3.12625E-4	0.0977	0.42446	8.60084E-5
2.4	9.25943E-5	0.09358	0.42912	8.77954E-5
2.6	1.28269E-5	0.08743	0.41377	9.09255E-5
2.8	2.35535E-4	0.08379	0.40785	9.30993E-5
3	0.00179	0.07959	0.38081	9.44677E-5
3.2	9.88094E-4	0.07348	0.34823	9.63502E-5
3.4	5.24664E-4	0.06906	0.31558	9.16657E-5
3.6	7.66005E-4	0.06438	0.26552	8.48152E-5
3.8	6.29881E-5	0.06001	0.21781	7.55721E-5
4	3.96934E-4	0.05734	0.173	6.3591E-5
4.2	5.12218E-4	0.05436	0.12489	5.08518E-5
4.4	4.74341E-6	0.05117	0.08454	3.87456E-5
4.6	1.99302E-7	0.04934	0.06007	2.78669E-5
4.8	0.00454	0.05215	0.04213	1.96331E-5
5	4.126E-5	0.04761	0.04755	1.29493E-5
5.2	0.005	0.05044	0.04508	9.0294E-6
5.4	0.01	0.05138	0.05563	6.62853E-6
5.6	8.16633E-5	0.10864	0.42269	8.61915E-5

Table S9. Best-fitting parameters of the generalized single Debye model for the frequency dependence of the out-of-phase molar magnetic susceptibility (χ'') as a function of the temperature for **{2-Nd$_2$}** (H_{dc} = 2200 Oe).

T / K	χ_s / cm^3 mol^{-1}	χ_t / cm^3 mol^{-1}	α	τ / s
1.8	0.00446	0.11437	0.13922	1.44957E-4
2	0.01484	0.1217	0.13324	1.31826E-4
2.2	2.63847E-5	0.10522	0.14481	1.16839E-4
2.4	0.00208	0.10517	0.15592	1.03597E-4
2.6	7.44116E-5	0.10222	0.17622	9.02279E-5
2.8	4.10429E-5	0.09807	0.17458	7.67977E-5
3	5.824E-4	0.09641	0.18527	7.49687E-5
3.2	9.07882E-5	0.09346	0.19173	6.77536E-5
3.4	3.0048E-5	0.08986	0.18924	6.30861E-5
3.6	1.29367E-5	0.08612	0.18289	5.85901E-5
3.8	3.72409E-5	0.08345	0.17948	5.09193E-5
4	1.68093E-4	0.07801	0.15064	5.00945E-5
4.2	2.74396E-4	0.07485	0.13826	4.62849E-5
4.4	0.00148	0.07283	0.12428	4.25622E-5
4.6	4.34814E-4	0.06864	0.10726	3.84366E-5
4.8	0.00211	0.06799	0.09109	3.42219E-5
5	0.00246	0.06567	0.08136	2.90943E-5
5.2	0.00475	0.06536	0.0629	2.74024E-5
5.4	0.00481	0.06238	0.04792	2.41691E-5
5.6	0.00653	0.06372	0.05043	2.06952E-5
5.8	1.05785E-4	0.05526	0.03766	1.79985E-5
6	0.00492	0.05953	0.04051	1.42471E-5

Table S10. Summary of the best-fitting parameters of the temperature dependence of the relaxation time of magnetization (τ) of **{1-Nd$_2$}** (H_{dc} = 2400 Oe) and **{2-Nd$_2$}** (H_{dc} = 2200 Oe).

Mechanism	Parameter	{1-Nd$_2$}	{2-Nd$_2$}
QTM	τ_{QTM}	1.05 10^{-4} s	1.34 10^{-4} s
Raman	C	0.051 s^{-1} K^{-n}	56.8 s^{-1} K^{-n}
	n	8.66	3.83

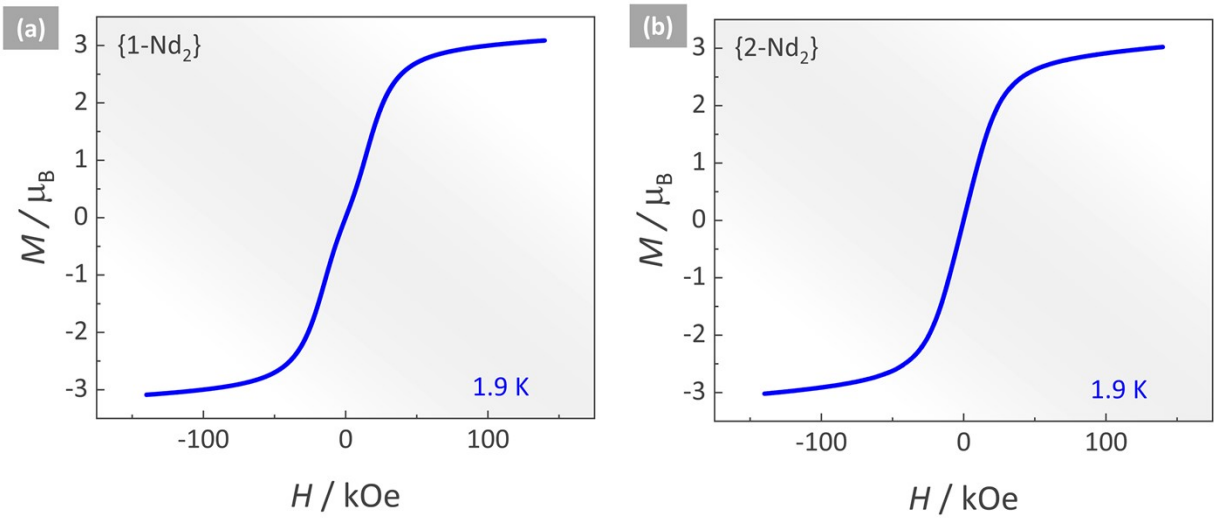

Fig. S10. Magnetic hysteresis at 1.9 K for **{1-Nd$_2$}** and **{2-Nd$_2$}**. No retention of the magnetization is observed.

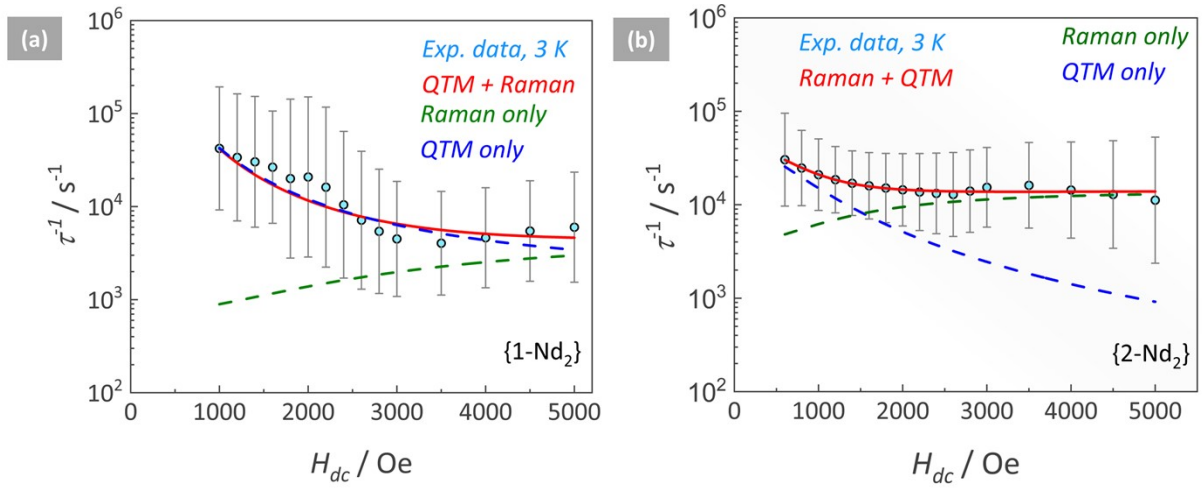

Fig. S11. Comparison of the field dependence of the relaxation time of magnetization (τ) at 3 K for (a) **{1-Nd$_2$}** and (b) **{2-Nd$_2$}**. The solid lines represent the best fit to a combination of QTM and Raman mechanisms.

Supplementary Note S5 – Additional Luminescence Data

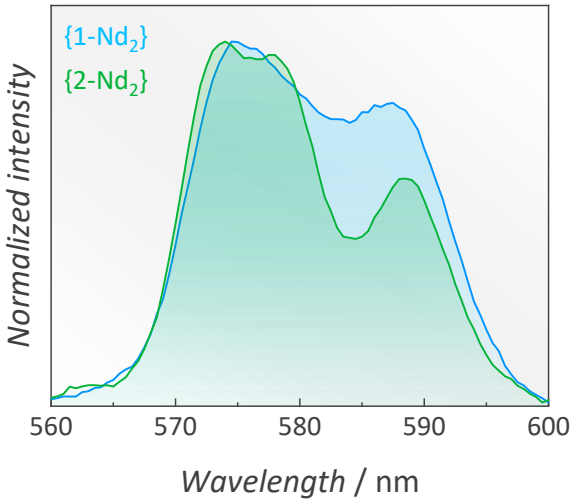

Fig. S12. Excitation (λ_{em} = 1060 nm, 10 K) spectra of **{1-Nd$_2$}** and **{2-Nd$_2$}** crushed crystals within the 560 – 600 nm spectral range assigned to the $^4I_{9/2} \rightarrow {}^4G_{5/2} + {}^2G_{7/2}$ transitions.

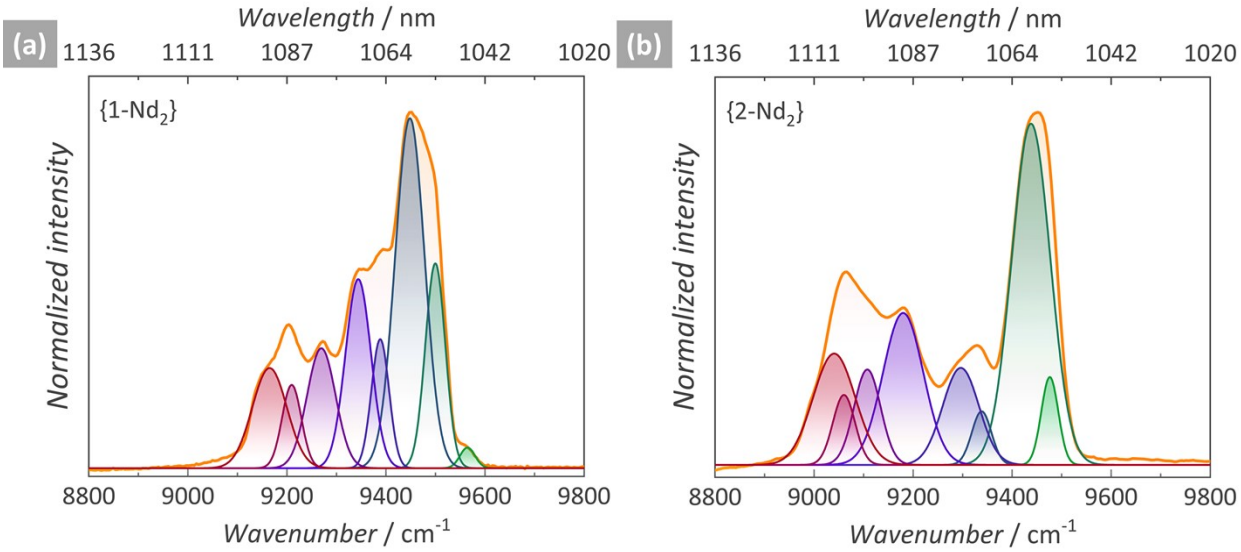

Fig. S13. Deconvolution of the emission spectrum of (a) **{1-Nd$_2$}** and (b) **{2-Nd$_2$}** crushed crystals measured at 10 K by applying a gaussian function ($R^2 > 0.99$) monitoring the $^4F_{3/2} \rightarrow {}^4I_{11/2}$ transition region.

Supplementary references

[1] J. Long, F. Habib, P-H. Lin, I. Korobkov, G. Enright, L. Ungur, W. Wernsdorfer, L. F. Chibotaru, M. Murugesu Single-Molecule Magnet Behavior for an Antiferromagnetically Superexchange-Coupled Dinuclear Dysprosium(III) Complex. *J. Am. Chem. Soc. 2011*, **133**, 5319.

[2] APEX Software Suite v 2010 Bruker AXS Inc. Madison Wisconsin USA, **2010**.

[3] R. H. Blessing, An empirical correction for absorption anisotropy. *Acta Crystallogr. Sect. A* 1995, **A51**, 33.

[4] G. M. Sheldrick, A short history of SHELX. *Acta Crystallogr. A.* 2008 **A*64***, 112.

[5] C. B. Hübschle, G. M. Sheldrick, B. Dittrich, ShelXle: a Qt graphical user interface for SHELXL. *J. Appl. Crystallogr.* 2011, **44**, 1281.

[6] C. D. S. Brites, A. Millán, L. D. Carlos, Lanthanides in Luminescent Thermometry. In: Handbook on the Physics and Chemistry of Rare Earths; Elsevier, 2016; pp 339-427.